

Coexistence of gapless excitations and commensurate charge-density wave in the 2H-transition metal dichalcogenides

Ryan L. Barnett,¹ Anatoli Polkovnikov,¹ Eugene Demler,¹ Wei-Guo Yin,² and Wei Ku²

¹*Department of Physics, Harvard University, Cambridge, MA 02138*

²*Physics Department, Brookhaven National Laboratory, Upton, NY 11973*

(Dated: November 14, 2018)

An unexpected feature common to 2H-transition metal dichalcogenides (2H-TMDs) is revealed with first-principles Wannier functions analysis of the electronic structure of the prototype 2H-TaSe₂: The low-energy Ta “ $5d_{z^2}$ ” bands governing the physics of charge-density wave (CDW) is dominated by hopping between next-nearest neighbors. With this motivation we develop a minimal effective model for the CDW formation, in which the unusual form of the hopping leads to an approximate decoupling of the three sublattices. In the CDW phase one sublattice remains undistorted, leaving the bands associated with it ungapped everywhere in the Fermi surface, resolving the long-standing puzzle of coexistence of gapless excitations and commensurate CDW in the 2H-TMDs.

PACS numbers: 71.45.Lr, 71.20.-b, 71.18.+y

Charge-density waves (CDWs) in solids has been a topic of central interest in condensed matter physics for many years [1]. Recent scanning tunneling microscopy experiments showing a periodic modulation in the local density of states in cuprate superconductors [2, 3], has reinvigorated such interest. Despite being one of the earliest discovered class of materials which exhibit a CDW at low temperatures [4], many properties of the 2H-transition metal dichalcogenides (2H-TMDs) are still not understood, leading to much recent theoretical [5, 6, 7] and experimental [8, 9, 10, 11, 12, 13, 14, 15] research effort (for a review, see Ref. [16]). Two key issues concerning the CDW phase in these materials deserve the most attention. First, controversy exists between different experimental groups on the driving mechanism of CDW originating from quantitative differences between the angle-resolved photoemission spectroscopy (ARPES) data. While some experimental results [9, 10, 11, 12] suggest that the hexagonal Fermi surfaces around the Γ point are consistent with the CDW nesting vector, others [13, 14, 15] indicate that this Fermi surface is too large to give the correct nesting vector. Second, and of a more qualitative nature, ARPES measurements [9, 10, 11, 12, 13, 14, 15] find no evidence of a gap opening on the hexagonal Fermi surface, in direct contrast with traditional wisdom of CDW materials.

In this Letter, we focus on the latter issue and suggest a simple picture for why such gapless excitations are permitted in the CDW phase. Using density-functional theory, the electronic structure of prototype 2H-TMD, 2H-TaSe₂, is analyzed with a newly developed Wannier function (WF) approach [17, 18], and a striking feature is revealed: the low-energy bands near Fermi surfaces, which governs the physics of CDW, is dominated by hopping between second-nearest neighbors. This special nature of hopping, in combination with the triangular lattice vectors, effectively splits the system into three weakly coupled triangular sublattices. Since the CDW

state gives distortion of only two of the sublattices, whose stability is illustrated with a simple model, such unique electronic structure naturally leaves the bands associated with the undistorted sublattice ungapped in this CDW phase, resolving the puzzle of the observed gapless excitations along the nested regions of the Fermi surface.

The lattice structure of 2H-TMDs consists of stacked layers of 2D-triangular lattices of transition metals (e.g. Ta or Nb) sandwiched between layers of chalcogen atoms (e.g. S or Se). Rough estimation of the ionization leads to the Ta⁴⁺Se²⁻ configuration with one valence $5d_{z^2}$ electron left per Ta atom that forms the metallic bands at the Fermi level. Indeed, the band structure from our first-principles calculations [19] (see Fig. 1) shows a strong d_{z^2} character in the two metallic bands corresponding to two weakly coupled TaSe₂ sandwiches per unit cell. Unexpectedly, little Se p characters are found in these two bands. The calculated low-energy bands agree well with experiments, except that the saddle bands on the Γ K and Γ H lines are not as flat and close to the Fermi level as

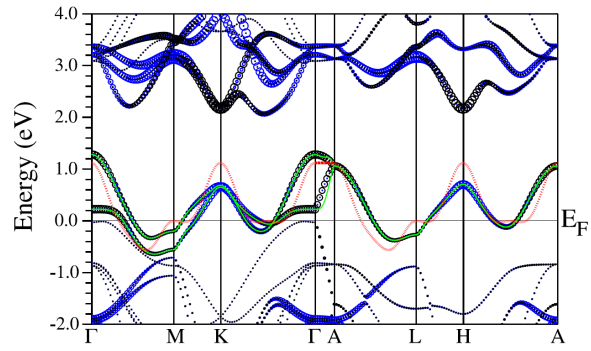


FIG. 1: First-principles band structure (dots) with the d_{z^2} (black circles) and $d_{xy}/d_{x^2-y^2}$ (blue circles) characters shown. The bands below -0.7 eV are mainly Se p bands. Also shown are the bands constructed from low-energy WFs (green solid lines) and a 2D ‘nesting’ model (red dotted line; see text).

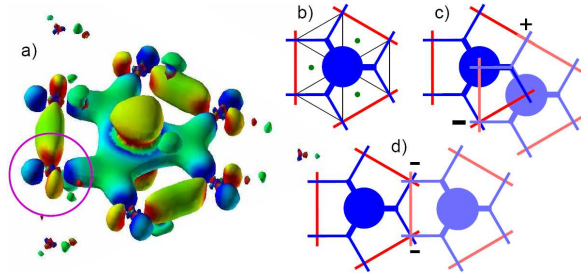


FIG. 2: a) Low-energy WF centered at Ta sites with a_g (d_{z^2}) symmetry, colored to show its gradient from positive (red) to negative (blue). Notice the local $d_{xy}/d_{x^2-y^2}$ symmetry in the hybridization tail (circled) located at neighboring Ta sites. b) Schematics of the WF in the layer of the Ta triangular lattice, with a similar color scheme giving the sign of the WF and three small dots marking the positions of Se atoms in the next layer. c) and d) Schematics of phase interference in hopping to first and second nearest neighbors, respectively.

reported [9, 11].

Based on the first-principles ground state, the low-energy Hilbert space can be accurately extracted via local WFs (see Fig. 2), which we constructed by extending recently developed energy-resolved method [17, 18] to incorporate desired symmetry [21]. As expected, the WF located at each Ta site has strong d_{z^2} symmetry near the center, before extending its *unusual tails* of $d_{xy}/d_{x^2-y^2}$ symmetry to the nearest neighboring Ta sites due to strong hybridization with the $d_{xy}/d_{x^2-y^2}$ orbitals near the K and H points (see Fig. 1). This particular shape of the WF results in an intriguing feature in the hopping integral (evaluated via $t_{\mu\nu} = \langle \mu | h^{DFT} | \nu \rangle$ with density functional theory Hamiltonian, h^{DFT} , and Wannier states $|\mu\rangle$ and $|\nu\rangle$). That is, the second neighbor hopping, $t_2 = 115$ meV, overwhelms the first neighbor hopping, $t_1 = 38$ meV, due to remarkable phase cancelation in the latter case (to be discussed in more detail below). In addition, interlayer hoppings are found to be comparable to first-neighbor in-plane hopping with $t_{\perp,1} = 29$ meV and $t_{\perp,2} = 23$ meV.

A simple microscopic picture for the unexpected dominance of second-neighbor hopping can be obtained from the symmetry of the WFs. As shown in Fig. 2(c) and (d), the contributions to the hopping parameters between neighboring WFs come mainly from overlap of their hybridization tails, since the tail-center ($d_{z^2} - d_{xy}/d_{x^2-y^2}$) overlap gives negligible contribution due to its odd parity. While the first-neighbor hopping suffers seriously from the phase cancelation (illustrated by the *opposite* sign in Fig. 2(c)), the second-neighbor hopping benefits greatly from the phase coherence (the same sign in Fig. 2(d)) of the overlap. Such symmetry consideration should hold for all 2H-TMDs of the same class, due to their similar local environment around the transition metal sites.

Specifically in 2H-TaSe₂, this unusual electronic struc-

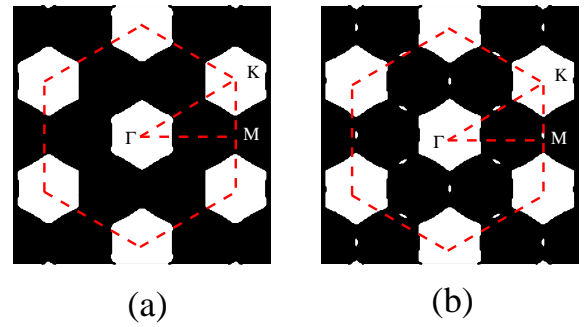


FIG. 3: (a) The Fermi surface from the tight-binding band structure. White indicates unoccupied states and black indicates occupied states. (b) The Fermi surface for a slightly smaller chemical potential showing the extended saddle bands (small white regions). The first Brillouin zone is the hexagonal cell formed by the red dashed lines.

ture provides a plausible intuitive resolution to the puzzling experimental observation of gapless excitations in the CDW phase. Indeed, with the dominating second neighbor hopping in a triangular lattice, the system effectively splits into *three* weakly coupled sublattices. As we discuss below, one of the sublattices remains undistorted in the CDW phase (see Fig. 4) and therefore the bands associated with it are ungapped.

With the dominance of the second neighbor hopping established, we now move on to construct a minimal, ‘nesting’ model which captures the essential physics of the gapless CDW in 2H-TMDs. We start with the simple 2D tight-binding energies given by

$$\varepsilon_{\mathbf{k}}^0 = \sum_{\mathbf{R}} t_{|\mathbf{R}|} \cos(\mathbf{k} \cdot \mathbf{R}) \quad (1)$$

where \mathbf{R} runs over the triangular lattice defined by lattice vectors $\mathbf{a}_1 = a(\sqrt{3}/2, 1/2)$ and $\mathbf{a}_2 = a(\sqrt{3}/2, -1/2)$. In addition to t_2 , $t_6 = t_2/3$ [22] (all other hoppings neglected) is introduced to produce the Fermi surface of an almost perfectly nested “hexagonal checkerboard” pattern similar to the recent ARPES data with extended saddle bands (very close to but below the Fermi energy for extended regions along ΓK) [9, 10, 11, 12], as shown in Fig. 3. The corresponding band (with t_2 adjusted to 140 meV) compares reasonably well with the first principles results (see Fig. 1; the two metallic bands are degenerate in the 2D model). As we show below, *even with such a perfect Fermi surface nesting, no gap is opened upon the formation of CDW*.

Continuing the development of our minimal model, we next consider the CDW lattice distortions. The detailed neutron diffraction experiments of Moncton *et al.* [23] have determined that the ionic displacements have Σ_1 symmetry, which corresponds to longitudinal motion of the Ta atoms in the basal plane with amplitude given by experiment. However, the fitting procedure to the

measured geometric structure factors was insensitive to the overall phase φ of the distortions. Following this work, the atomic displacements having Σ_1 symmetry corresponding to the triple period CDW in the 2H-TMDs are given by

$$\delta\mathbf{R} = \sum_{\mathbf{Q}} u \cos(\mathbf{Q} \cdot \mathbf{R} + \varphi) \hat{\mathbf{Q}}. \quad (2)$$

Here u is the amplitude and the sum runs over the vectors $\mathbf{Q}_1 = \mathbf{b}_1/3$, $\mathbf{Q}_2 = \mathbf{b}_2/3$, and $\mathbf{Q}_3 = -(\mathbf{b}_1 + \mathbf{b}_2)/3$, where the reciprocal lattice vectors are given by $\mathbf{b}_1 = \frac{2\pi}{a}(1/\sqrt{3}, 1)$ and $\mathbf{b}_2 = \frac{2\pi}{a}(1/\sqrt{3}, -1)$. The above atomic displacements also splits the lattice into three independent sublattices, where one of these sublattices does not experience displacements for any φ . We will determine the overall phase factor φ by minimizing the total energy. It can be seen that the magnitude of the displacements given by Eq. (2) will not depend on φ . Thus the elastic energy of the system will not depend on the phase of the CDW for this model system and our problem is reduced to finding the phase that minimizes the energy of the conduction band. Expanding the crystal potential to first order in $\delta\mathbf{R}$ given by Eq. (2) leads to the perturbation

$$\mathcal{H}' = \sum_{\mathbf{k}, \mathbf{Q}} \Delta_{\mathbf{k}}^{\mathbf{Q}} c_{\mathbf{k}}^{\dagger} c_{\mathbf{k}+\mathbf{Q}} + \text{h.c.} \quad (3)$$

where the wave vector \mathbf{k} is summed over the first Brillouin zone. For simplicity, we assume that the change in the hopping parameters due to the lattice distortion is proportional to the change in the absolute distance between neighboring atoms: $\delta t_{\mathbf{R}\mathbf{R}'} \propto (\delta\mathbf{R} - \delta\mathbf{R}') \cdot (\mathbf{R} - \mathbf{R}')$. Then

$$\Delta_{\mathbf{k}}^{\mathbf{Q}} = -ue^{-i\varphi} \sum_{\mathbf{R}} \gamma_{|\mathbf{R}|} (e^{-i\mathbf{Q} \cdot \mathbf{R}} - 1) e^{-i\mathbf{k} \cdot \mathbf{R}} \hat{\mathbf{Q}} \cdot \hat{\mathbf{R}} \quad (4)$$

where the lattice vector \mathbf{R} is summed over the *second* nearest neighbors to the atom at the origin and $\gamma_{|\mathbf{R}|=2} > 0$ is the electron-phonon coupling constant in the unit of energy/distance. Since the unit cell of the distorted lattice contains nine sites of the original lattice, the renormalized energies $\varepsilon_{\mathbf{k}}^{(n)}$ are given by the eigenvalues of a 9×9 matrix which is rather cumbersome and we will give its explicit expression elsewhere.

We can now write the total energy as a function of the amplitude and phase of the distortion as

$$E_{\text{tot}}(u, \varphi) = \int_{-\infty}^{\mu} \varepsilon \rho(\varepsilon) d\varepsilon + E_{\text{el}}(u) \quad (5)$$

where $\rho(\varepsilon) = \sum_{\mathbf{k}, n} \delta(\varepsilon - \varepsilon_{\mathbf{k}}^{(n)})$ is the density of electronic states and $E_{\text{el}}(u)$ is the elastic energy which, as we noted before, is independent of the phase of the distortion. The \mathbf{k} -integration is performed by using a fine Monkhorst-Pack mesh and corresponding weights [24] in

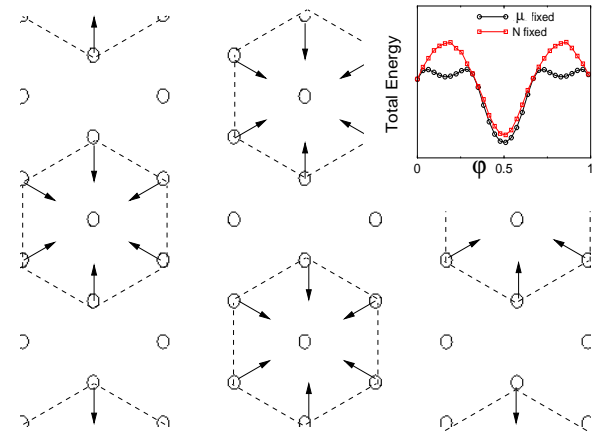


FIG. 4: Atomic displacement pattern corresponding to the phase $\varphi = \pi/2$ in Eq. (2). The inset shows the total energy of the CDW state as the function of phase φ where the total energy units are arbitrary and the phase is in units of π .

the irreducible Brillouin zone of the triangular lattice. We determine the chemical potential μ by considering two extreme cases: (i) Fixed particle number N , which corresponds to an isolated metallic band at the Fermi energy. (ii) Fixed $\mu = 0$, which corresponds to significant spectral weight from the other bands at the Fermi energy. The realistic situation, with two metallic bands at the Fermi energy arising from the multi-layer structure should reside somewhere between these two extremes. We find that the unanimous minimum for both extreme cases occurs when $\varphi = \pi/2$. This minimum will become more pronounced with increased electron-phonon coupling constant. In Fig. 4 we show the corresponding atomic displacement pattern, which is consistent with the charge maxima seen in scanning tunneling microscopy experiments [25, 26]. Furthermore, to check the robustness of this result, we have performed the same calculation, but with t_6 set to zero, and have found that the minimal total energy still occurs at $\varphi = \pi/2$.

Now that the phase of the CDW has been determined we will analyze the renormalized quasiparticle dispersion in the presence of the CDW. The energy spectrum from the undistorted sublattice is shown in Fig. 5(a) and that from distorted sublattices is shown in Fig. 5(b) along the Γ -M direction, which is along the nested region of the Γ -centered hexagonal Fermi surface. Clearly, those associated with the undistorted sublattice do not change [Fig. 5(a)]. Thus, the corresponding sub-bands remain metallic in the CDW phase. On the other hand, the bands originating from the two distorted sublattices are doubly degenerate and we find a gap opens at the Fermi energy [Fig. 5(b)]. Moreover, to make comparison with experiment more direct, in Fig. 5(c) and Fig. 5(d) we present theoretical ARPES spectra $A(\mathbf{k}, \omega) = \frac{1}{\pi} f(\omega) \text{Im}G(\mathbf{k}, \omega)$ where $G(\mathbf{k}, \omega)$ is the single particle Green's function and $f(\omega)$ is the Fermi distribu-

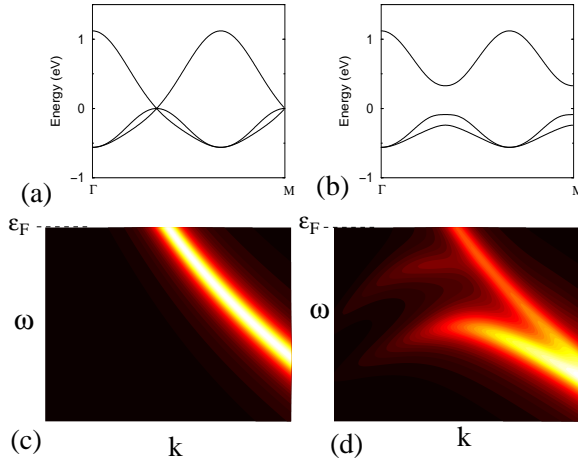


FIG. 5: The bands in the low temperature CDW state originating from the undistorted (a) and distorted (b) sublattices. The increase in the number of bands corresponds to backfolding resulting from the 3×3 supercell. Theoretical ARPES spectra for the normal (c) (corresponding to vanishing electron-phonon coupling) and CDW (d) states for wave vectors over the nested region of the Fermi energy along Γ M. The energy range is -0.47 to 0 eV relative to the Fermi energy and the momentum range is $\frac{\mathbf{b}_1 + \mathbf{b}_2}{3}, \frac{3}{10}$ to $\frac{\mathbf{b}_1 + \mathbf{b}_2}{3}, \frac{7}{10}$.

tion function for wave vectors in a small region of the nested portion of the Fermi surface. To emulate experimental data, we have chosen a broadening of $\eta = 40$ meV of the spectral density function. In Fig. 5(b) both the gapped and ungapped bands are visible (for an account of the weightings of satellite bands in CDW materials, see Voit *et al.* [27]). The most direct comparison between experimental data is with the work of Valla *et al.* [13] where there is a plot similar to Fig. 5(a). It is also shown in this paper that no gap opens along FK, being consistent with Fig. 5(b).

A question that naturally follows is, how robust this result is when the finite first neighbor interaction—which mixes all bands and thus destroys the exact decoupling into the three independent sublattices—is taken into account. We examine this issue, switching on the first-neighbor electron-phonon coupling constant γ_1 in Eq. (4), up to a third of the value of γ_2 as suggested by the first principles results: $t_1 \simeq t_2/3$. As expected, we find that the degeneracy of the bands originating from the distorted sublattices shown in Fig. 5(b) is lifted. In addition, the triple degeneracy originating from the undistorted sublattice shown in Fig. 5(a) at the Fermi energy is lifted. However, this does *not* produce a quasiparticle gap at the Fermi energy. More specifically, this triple degeneracy is lifted in such a way that two of the energies are increased to above the Fermi energy and the other one is decreased to below the Fermi energy. It can be seen that this will indeed not gap the Fermi surface, given γ_1 is considerably smaller than γ_2 .

In conclusion, we have studied the CDW state in the 2H-transition metal dichalcogenides and found that due to a unique feature in the electronic structure of these materials revealed from first-principles calculations, the triangular lattice can be effectively decoupled into three independent sublattices, with one remaining undistorted in the CDW phase. As illustrated with a model calculation, this leads to the remarkable situation where no regions of the entire Fermi surface become gapped even when these materials exhibit a commensurate CDW.

The work done at Harvard University was supported by the NSF (DMR-0132874, DMR-0231631), the Sloan Foundation, and Harvard NSEC and MRSEC (DMR-0213805). The work done at Brookhaven National Laboratory was supported by U.S. Department of Energy under Contract No. DE-AC02-98CH1-886 and DOE-CMSN. W.Y. and W.K. thank A.M. Tsvelik and T. Valla for helpful discussions.

- [1] G. Grüner, *Density Waves in Solids* (Perseus Publishing, 1994).
- [2] C. Howald, H. Eisaki, N. Kaneko, M. Greven, and A. Kapitulnik, Phys. Rev. B **67**, 014533 (2003).
- [3] T. Hanaguri, C. Lupien, Y. Kohsaka, D.H. Lee, M. Azuma, M. Takano, H. Takagi, and J.C. Davis, Nature **430**, 1001 (2004).
- [4] J. A. Wilson, F. J. D. Salvo, and S. Mahajan, Phys. Rev. Lett. **32**, 882 (1974).
- [5] T. M. Rice and G. K. Scott, Phys. Rev. Lett. **35**, 120 (1975).
- [6] A. H. CastroNeto, Phys. Rev. Lett. **86**, 4382 (2001).
- [7] B. Uchoa, G. G. Cabrera, and A. H. C. Neto (2004).
- [8] T. Yokoya, T. Kiss, A. Chainani, S. Shin, M. Nohara, and H. Takagi, Science **294**, 2518 (2001).
- [9] R. Liu, C. G. Olson, W. C. Tonjes, and R. F. Frindt, Phys. Rev. Lett. **80**, 5762 (1998), and references therein.
- [10] T. Straub, T. Finteis, R. Claessen, P. Steiner, S. Hufner, P. Blaha, C. S. Oglesby, and E. Bucher, Phys. Rev. Lett. **82**, 4504 (1999).
- [11] R. Liu, W. C. Tonjes, V. A. Greanya, C. G. Olson, and R. F. Frindt, Phys. Rev. B **61**, 5212 (2000).
- [12] W. C. Tonjes, V. A. Greanya, R. Liu, C. G. Olson, and P. Molinie, Phys. Rev. B **63**, 235101 (2001).
- [13] T. Valla, A. V. Fedorov, P. D. Johnson, J. Xue, K. E. Smith, and F. J. DiSalvo, Phys. Rev. Lett. **85**, 4759 (2000).
- [14] K. Rossnagel, O. Seifarth, L. Kipp, M. Skibowski, D. Voss, P. Kruger, A. Mazur, and J. Pollmann, Phys. Rev. B **64**, 235119 (2001).
- [15] T. Valla, A. V. Fedorov, P. D. Johnson, P. A. Glans, C. McGuinness, K. E. Smith, E. Y. Andrei, and H. Berger, Phys. Rev. Lett. **92**, 086401 (2004).
- [16] R. L. Withers and J. A. Wilson, J. Phys. C **19**, 4809 (1986).
- [17] W. Ku, H. Rosner, W. E. Pickett, and R. T. Scalettar, Phys. Rev. Lett. **89**, 167204 (2002).
- [18] S. Grenier, J. P. Hill, V. Kiryukhin, W. Ku, Y.-J. Kim, K. J. Thomas, S.-W. Cheong, Y. Tokura, Y. Tomioka,

D. Casa, *et al.*, Phys. Rev. Lett **94**, 047203 (2005).

[19] We applied the WIEN2k [20] implementation of the full potential linearized augmented plane wave method in the local density approximation of density functional theory with the crystallographic data [23]. The basis size was determined by $R_{mt}K_{max} = 7$ and the Brillouin zone was sampled with a regular mesh containing 99 irreducible k -points to achieve energy convergence of 1 meV.

[20] P. Blaha *et al.*, Comput. Phys. Commun. **147**, 71 (2002).

[21] W. Ku, W. E. Pickett, , and R. Scalettar, to be published.

[22] t_6 calculated from first principles is vanishingly small.

[23] D. E. Moncton, J. D. Axe, and F. J. DiSalvo, Phys. Rev. B **16**, 801 (1977).

[24] H. J. Monkhorst and J. D. Pack, Phys. Rev. B **13**, 5188 (1976).

[25] C. G. Slough, W. W. McNairy, R. V. Coleman, B. Drake, and P. K. Hansma, Phys. Rev. B **34**, 994 (1986).

[26] R. V. Coleman, B. Giambattista, P. K. Hansma, A. Johnson, W. W. McNairy, and C. G. Slough, Adv. Phys. **37**, 559 (1988).

[27] J. Voint, L. Perfetti, F. Zwick, H. Berger, G. Margaritondo, G. Grüner, H. Hochst, and M. Grioni, Science **290**, 501 (2000).